Appl. Phys. B 77, 831–837 (2003)
DOI: 10.1007/s00340-003-1322-4

Applied Physics B
Lasers and Optics

O.V. CHUTKO[1]
V.M. GORDIENKO[1]
I.M. LACHKO[1]
B.V. MAR'IN[2]
A.B. SAVEL'EV[1,✉]
R.V. VOLKOV[1]

High-energy negative ions from expansion of high-temperature femtosecond laser plasma

[1] International Laser Center, Physics Faculty, M.V. Lomonosov Moscow State University, Vorob'evy gory, 119992 Moscow, Russia
[2] Institute of Nuclear Physics, M.V. Lomonosov Moscow State University, Vorob'evy gory, 119992 Moscow, Russia

Received: 22 April 2003/Revised version: 21 July 2003
Published online: 29 October 2003 •

ABSTRACT The atomic, charge and energy distributions of ions in expanding femtosecond laser plasmas have been studied by means of time-of-flight mass–charge spectroscopy. High-energy negative and positive ions with energies of up to 35 keV have been detected during the interaction of 200-fs laser pulses ($I \sim 2 \times 10^{16}$ W/cm^2) with silicon, titanium and other solid targets. A high correlation between negative and positive single-charged ions of the identical atomic number is shown. Negative ions are produced as a result of collisions of fast single-charged ions and neutrals with molecules of residual gas.

PACS 52.50.Jm; 52.70.Nc; 52.38.Ph

1 Introduction

Under appropriate conditions, many neutral atoms can form stable-state entities with additional electrons – the so-called negative ions [1, 2]. Fast negative ions prove valuable as the primary sources for particle accelerators [3, 4]. They can also be exploited for thin-film deposition and nanostructure formation [5] as well as for investigations of the behavior of negative clusters [5], etc.

As follows from the experimental data and results of numerical calculations, the yield of negative ions in dense plasmas reaches its maximum when the plasma temperature is of the order of the affinity energy, which depends on the atomic number of ion species and does not exceed a few eV [6]. In stationary low-temperature plasmas negative ions can be extracted by a strong electrostatic field; the kinetic energy of the ions, in this case, is proportional to the strength of the extracting field.

The formation of negative ions in the laser plasma blow-off during the interaction of nanosecond laser pulses with solid targets has been investigated during the past 15 years [5–9]. The investigations were carried out for low laser-pulse intensities (10^7–10^9 W/cm^2), when the plasma temperature is less than 10 eV and the average ionization state is near unity or even lower. Thus, the 'optimal' conditions for the production of negative ions were satisfied, but the plasma density was arbitrarily low. The yield, experimentally measured in [7] with the electrostatic extraction of ions, was about several percent of the total number of ions.

Negative ions can also be produced at higher laser-pulse intensities of 10^9–10^{10} W/cm^2, when initially hot (several tens of eV) plasma cools to the temperature of several eV due to the expansion into the vacuum [7]. In this case, negative ions can be easily separated from positive ions and neutrals by the mass-spectrometer separation technique, since kinetic energies of the ions reach 1 keV. Just as in the previous case, the number of negative ions is several percent of the total ion amount.

In [10], we reported the first experimental evidence of the formation of high-energy negative hydrogen ions during the blow-off of plasmas produced by a femtosecond laser pulse with an intensity of more than 10^{16} W/cm^2. The distinguishing feature of these negative ions is the extremely high kinetic energy, which reaches 35 keV for H^{1-} ions. In this paper, we present a detailed experimental study of the formation of high-energy negative ions under the interaction of a 200-fs laser pulse with a silicon target at intensities of more than 10^{14} W/cm^2.

2 Experimental setup

The schematic view of the experimental setup is shown in Fig. 1. A femtosecond dye laser system ($\lambda = 616$ nm, $\tau = 200$ fs, 1 Hz) was used to produce plasmas [11]. By focusing the laser pulse with a lens of $F/D \sim 6$, an intensity of 2×10^{16} W/cm^2 with a contrast higher than 10^5 was achieved at the target. A vacuum system included two chambers, the interaction and the registration ones, connected with each other by a short vacuum tube. Ion current measurements (described below) were conducted along with the hard X-ray yield measurements, thus allowing for the tight focusing and providing the estimation of the hot-electron temperature [12]. For the latter purpose, two NaJ(Tl) scintillation detectors supplied with special filter sets were used. They were placed approximately 10 degrees from the target normal and out of the plane of incidence of the laser light.

The measurements of the plasma blow-off were based on the mass–charge separation in the electrical field of a cylindrical analyzer performed simultaneously with the time-of-flight study [13]. It was accomplished by using a 180 degree

✉ Fax: +7-95/9393113, E-mail: savelev@femto.phys.msu.su

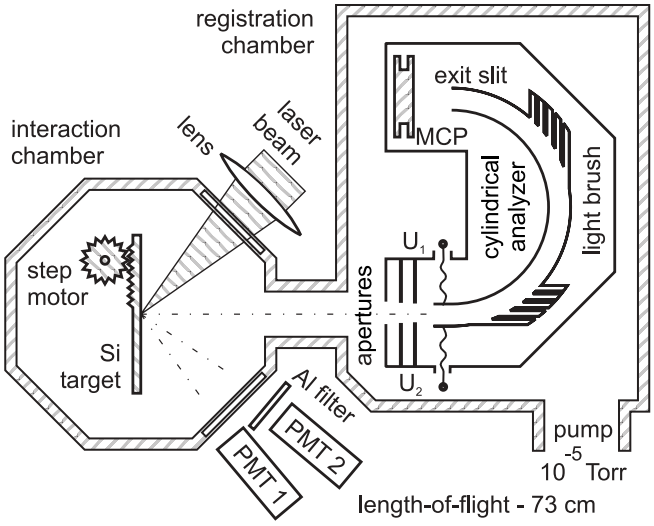

FIGURE 1 Schematic view of the experimental setup

semicylindrical electrostatic capacitor, each plate of which was kept at its own voltage (U_1 and U_2). The voltage difference between the plates (the deflecting voltage) could be varied within ± 8 kV, thus permitting the measurement of both positively and negatively charged particles. The analyzer was mounted in the registration chamber at 50-cm distance from the target normally to the target. The output current of the analyzer was registered by a chevron-type microchannel plate (MCP), which was placed at the exit slit of the analyzer plates. The signal from the MCP was coupled by a coaxial cable through a 50 Ohm impedance load to the input of a digital oscilloscope with 100-MHz bandwidth and 100-MHz sampling rate. Background gas pressure in the vacuum system required for the safe operation of the MCP was 1×10^{-5}–3×10^{-5} Torr.

The analyzer was calibrated by using a quasi-monochromatic glow cathode electron source. The energy of emitted electrons was established by applying the accelerating voltage to the ground and the grid. For each value of the accelerating voltage we obtained the corresponding values of the deflecting voltage and energy resolution. The dependences of both parameters on the accelerating voltage were well approximated by linear functions. Therefore, the energy of the detected particle ε with the charge Z was related to the deflecting voltage U as $\varepsilon = ZU/k$, where $k = (0.23 \pm 0.005)$ V/eV, while the relative energy resolution was independent of the particle energy and equal to $\pm 4\%$. It should be noted that the values of the relative energy resolution and coefficient k calculated from the analyzer geometry were, respectively, $\Delta\varepsilon/\varepsilon = \pm 5\%$ and $k = 0.2 \pm 0.01$ V/eV.

3 Results and discussion

A silicon target was chosen for our experiments since a body of data on plasmas produced by femtosecond laser pulses was obtained for targets of this very material. Figure 2 demonstrates typical time-of-flight traces of positive (Fig. 2a) and negative (Fig. 2b) particles, produced during the interaction of 200-fs pulses of the laser radiation with the 2×10^{16}-W/cm^2 intensity and 616-nm wavelength with the silicon target. Here, the deflecting voltage is $U = 1.05$ kV and MCP biasing is 1100 V for the detection of positive ions and 2600 V for the negative-ion detection. The recorded trace of positive ions contains usually a first high peak and a group of lower peaks. Knowing for a given trace the position of each peak on the time axis together with the deflecting voltage, we can determine the mass-to-charge ratio for the peak. Indeed, for the specified deflecting voltage U the time of flight of the detected ions is given by

$$t = l\sqrt{\frac{Mk}{2ZU}}, \tag{1}$$

where l is the length of flight defined as the sum of the distance from the target to the detector and the particle path inside the capacitor, M is the ion mass and Z is the ion charge.

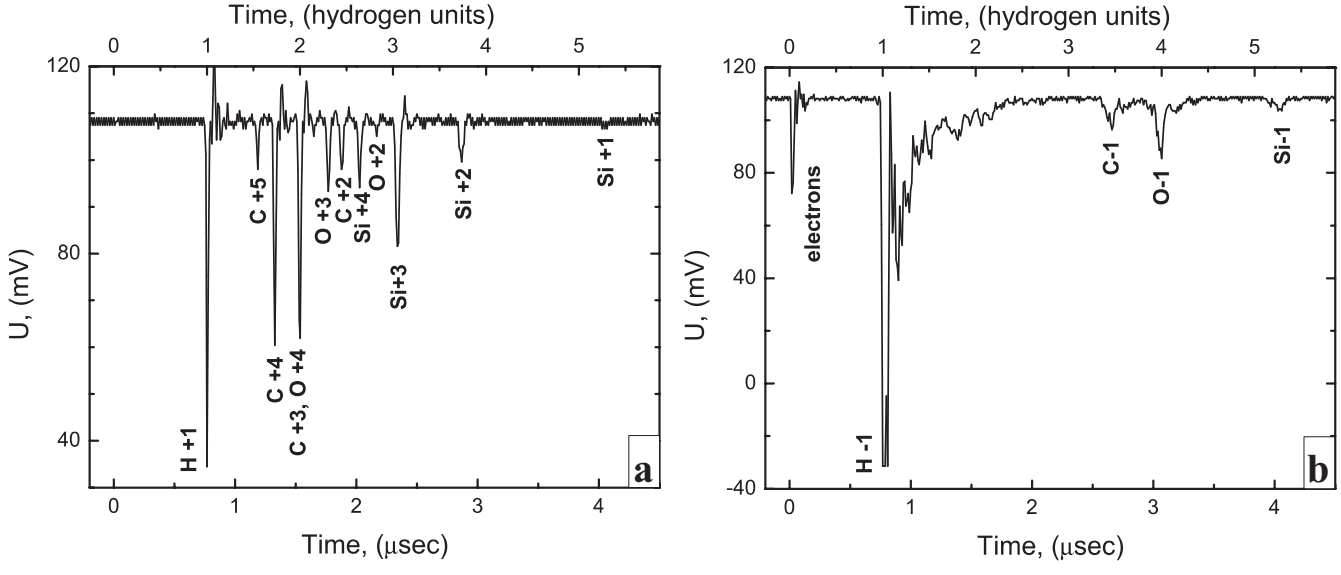

FIGURE 2 Time-of-flight single-shot spectra of positive (**a**) and negative (**b**) particles for $\varepsilon = 4.5\,Z$ keV

The data analysis of a single-shot trace has shown that the first high peak appearing at 0.1–1-μs delay (see Fig. 2a) is caused by the protons possessing the maximum Z/M value as compared with other ions. Figure 3 displays the dependence of the time of flight t for the first peak on the proton energy $\varepsilon_p = U/k$ (each point in Fig. 3 was obtained by averaging over 10 shots). The experimental data are well fitted by the function $\varepsilon^{-0.5}$ in accordance with (1). This fit allowed us to determine the length of flight as $l = 73 \pm 0.7$ cm.

The negative time-of-flight trace had an additional electron-caused peak located at the delay t of several tens of nanoseconds. The second peak in the negative trace and the proton peak in the positive trace measured for the same value of the deflecting voltage are situated at the same position on the time axis. Therefore, we can conclude that the second peak of the negative trace corresponds to the negatively charged hydrogen ions H^{-1}.

The origin of a group of peaks at longer delays t in both positive and negative traces is associated with the heavier ions of Si, C and O of different ionization states. Hydrogen, oxygen and carbon ions probably emanate from the impurities of the surface layer of the Si target (hydrocarbons, silicon dioxide, etc.). In Fig. 4, we have plotted the data on the charge state of positive plasma ions averaged over the entire range of deflecting voltage values, which is 0.1–8 kV (the results of 10 shots were stored for each voltage value). Unlabeled peaks correspond to artifacts arising due to the imperfect biasing of the MCP detector. The maximum charge state registered in this study was +6 for Si, +4 for O and +6 for C.

Among negatively charged particles we observed H^{-1}, C^{-1}, O^{-1} and Si^{-1} ions (see Fig. 4b). Since the energy E_a of electron affinity ranges from 0.754 eV for H^{-1} to 1.482 eV for O^{-1} [2], negative ions can appear in cold, stationary, slightly ionized plasmas with the temperature $T \sim E_a$ [6]. In our conditions, it could happen only at certain time delays with respect to the plasma formation during the plasma cooling to temperatures less than 10 eV (see below for more details).

It should be noted that to detect the signal from negative particles the MCP amplification was increased by the factor of ~ 1000. Therefore, the ratio of negatively to positively charged ions was 10^{-2} to 10^{-3} in our case, reaching values obtained at the nanosecond laser-pulse irradiation [7].

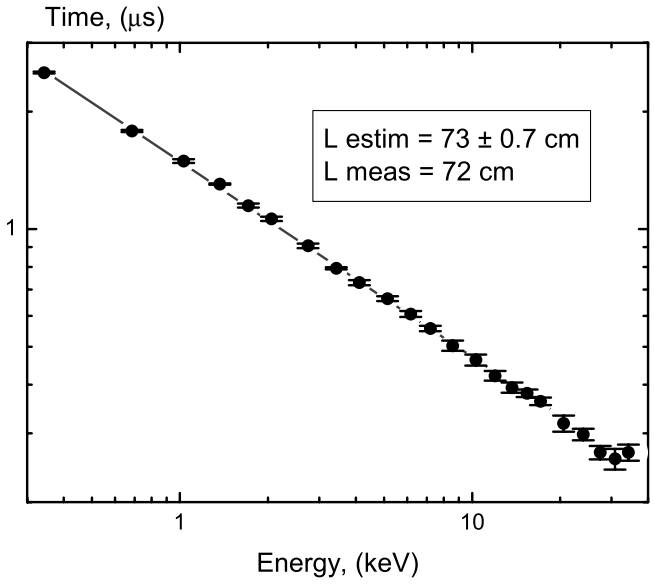

FIGURE 3 Time of appearance of first positive peak, supposed to be caused by protons, as a function of proton energy

Negative-ion peaks in Fig. 4b are much broader as compared with the similar peaks in Fig. 4a. The broad peak, corresponding to the detection of H^{-1} ions, has a complicated structure including an artifact at $Z/M \sim 1.3$ (the same particularity can be observed in Fig. 4a) and a long tail up to $Z/M \sim 5$, which seems to arise from the detection of slow electrons knocked out due to collisions of ions with the exit slit of the analyzer. These electrons are effectively detected because of low positive biasing of the input MCP plate.

Energy spectra of positive ions are shown in Fig. 5a–d for H, C, O and Si, respectively (each data point was obtained by averaging over 10 laser shots). The proton spectrum at energies of more than 3 keV can be well approximated by the exponential decay function with the 'temperature' $T_p \approx 8.5$ keV. Under our experimental conditions, this 'temperature' can be

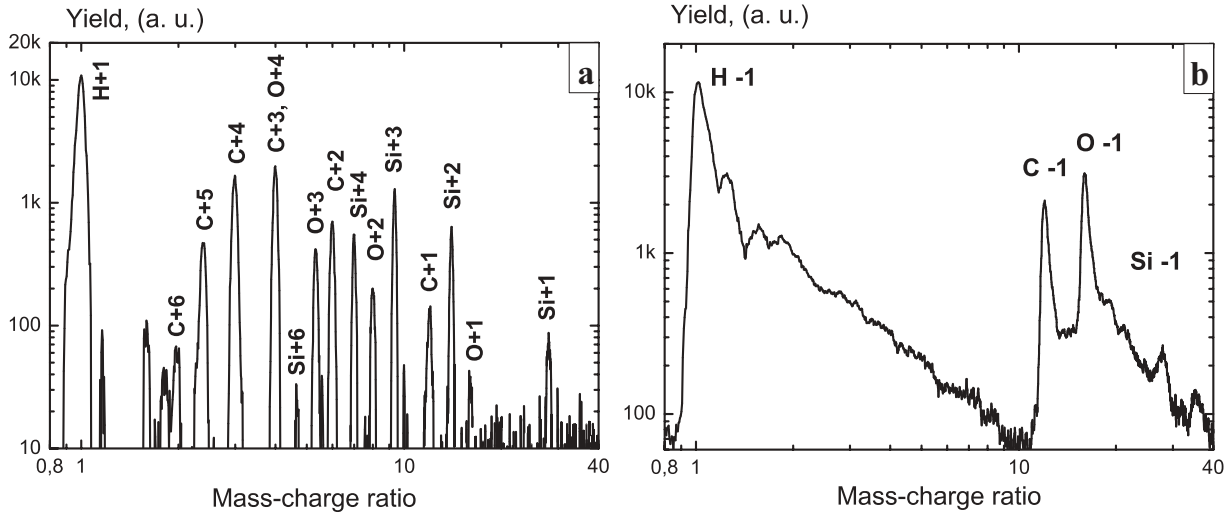

FIGURE 4 Mass-to-charge ratio spectra of positive (**a**) and negative (**b**) particles

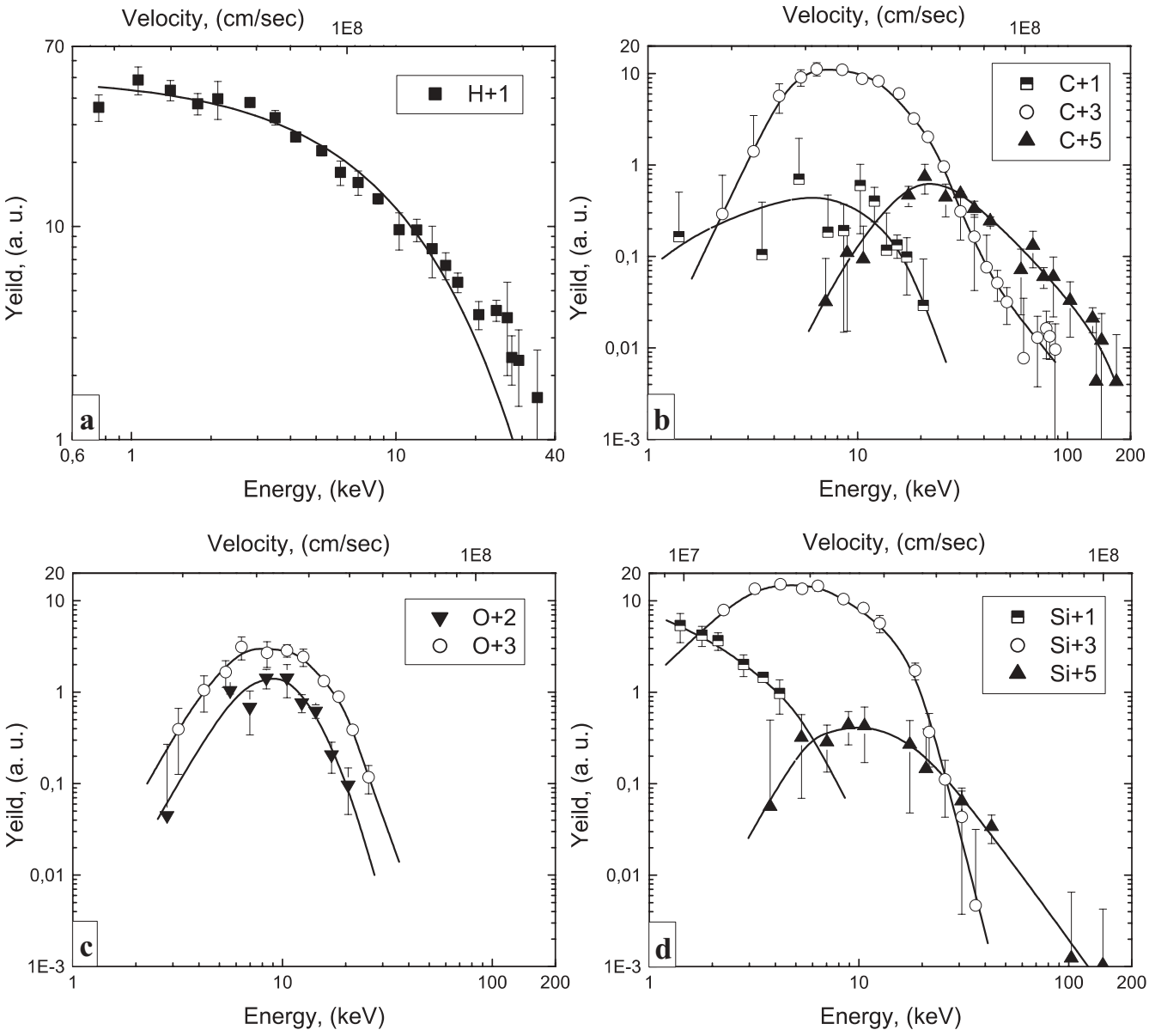

FIGURE 5 Energy spectra of H (**a**), C (**b**), O (**c**) and Si (**d**) ions (+1 – ■, +2 – ▼, +3 – ○, +5 – ▲ for $I \sim 10^{16}$ W/cm^2)

estimated as [14, 15]:

$$T_\mathrm{p} \approx m_\mathrm{e} c^2 \pi \sqrt{Q\delta R/\lambda} = 9\,\mathrm{keV}\,, \qquad (2)$$

where $\delta \sim 0.01$ is the coefficient determining the efficiency of the conversion of the laser energy into the energy of hot electrons, $Q = I\lambda^2/(5.48 \times 10^{18}\,\mathrm{W/cm^2\,\mu m^2}) \sim 0.0014$, m_e is the electron mass and $R \sim 1.5\,\mu$m is the radius of the focal spot.

We also estimated the mean energy of hot electrons by using the double-channel X-ray filter technique [12]. We measured the hard X-ray yield from plasma in each laser shot by two identical NaI(Tl) detectors supplied with different band filters. The ratio of signals from these detectors depends only on the hot-electron temperature (or the mean energy), which, consequently, can be estimated in each shot. Thus, the mean energy of hot electrons under our experimental conditions was estimated as $E_\mathrm{h} \approx 9 \pm 2$ keV. This value of E_h is in a reasonable agreement with the value $T_\mathrm{p} = 8.5$ keV, estimated from the slope of the proton spectrum in Fig. 5a. Hence, it can be concluded that under our conditions the fast-proton component is generated due to the spatial charge separation, caused by hot electrons escaping from plasma.

Spectra of 'heavy' C, O and Si ions shown in Fig. 5 have a more complicated structure and can hardly be approximated by a single-exponential function as in the case of protons. Nevertheless, the high-energy tail in these spectra can be well approximated by the exponential decay function with the 'temperature' of 6 ± 0.5 keV regardless of the atomic weight and charge of the ion. This 6-keV value for the slope of the high-energy tail of the ion spectra is slightly less than the value deduced from the proton spectrum (8.5 keV). It can be explained taking into account the higher mobility of the lightest hydrogen ion. Thanks to this fact the protons screen the electrostatic field generated by fast electrons from other ionic species.

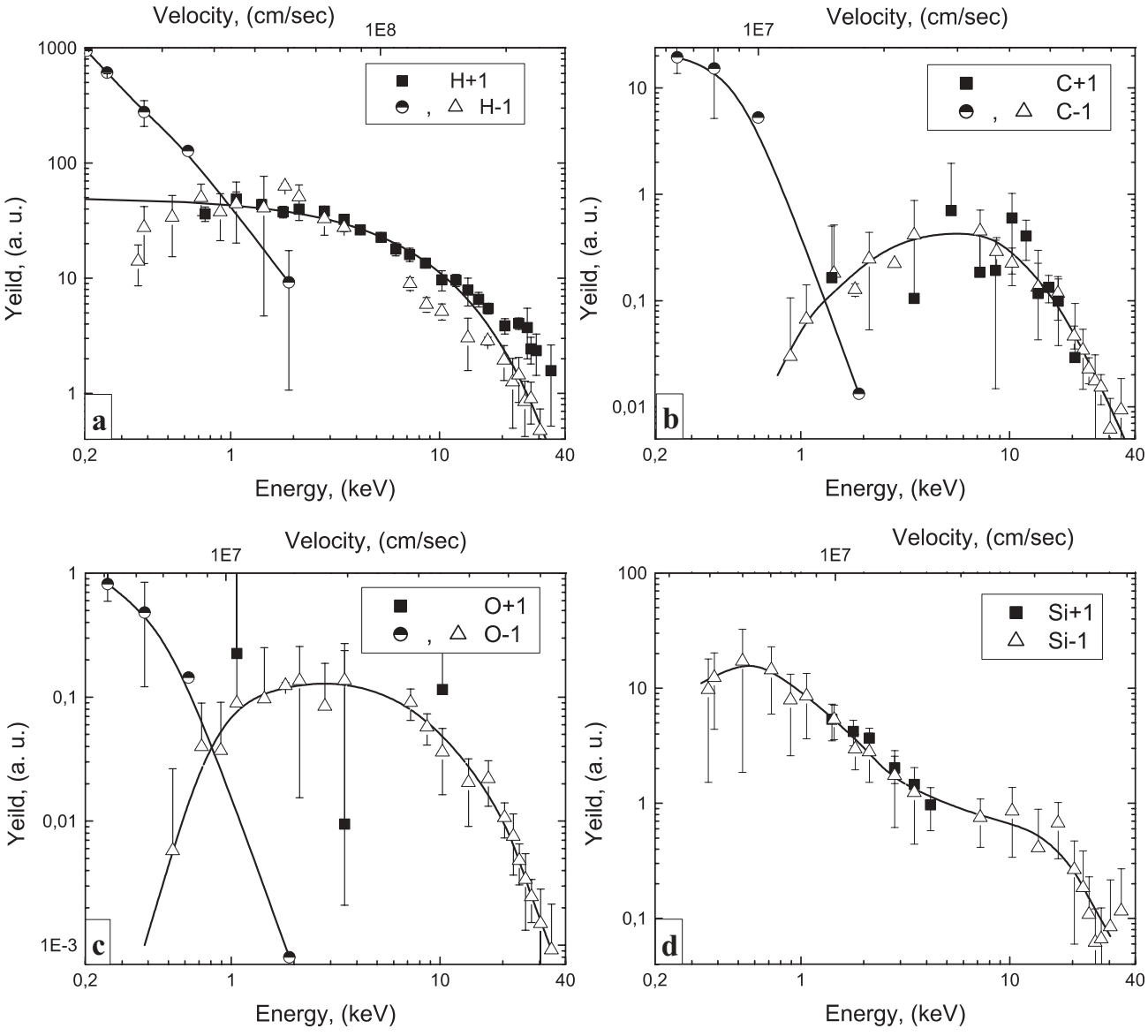

FIGURE 6 Spectra of positive and negative ions of H (**a**), C (**b**), O (**c**) and Si (**d**) (-1 – △, $+1$ – ■ at $I \sim 10^{16}$ W/cm^2 and ○– $I \sim 10^{15}$ W/cm^2). Explanations of the curves are given in the text

The distinguishing particularity of the obtained data is a high correlation between single-charged positive- and negative-ion spectra (see Fig. 6a–d): the spectrum of negative hydrogen ions also has the exponential high-energy tail with the 'temperature' of 7–8 keV and the maximum energy of negatively charged hydrogen ions is 35 keV. For single-charged carbon ions the spectral profiles of positive and negative ions are identical, with the broad maximum located near 5–7 keV. The same, though less pronounced (mostly due to the lack of data), particularities can be seen in O^{1+} and O^{1-} spectra. The spectral profiles of single-charged silicon ions (Fig. 6d) differ from those of other ionic species by the two lobes. Hence, negatively charged ions are likely produced from single-charged positive ions of the same atomic number. What is also important is that the amount of hydrogen negative ions is much higher than that of other negative-ion species.

The experiments at lower intensities of femtosecond laser pulses were performed as well. For the intensity of 10^{14} W/cm^2 we did not register any fast (with energies above 100 eV) negative ions, while the proton signal (with the ion energy less than 0.5 keV) became weaker but still was easily detectable. For the intensity of 10^{15} W/cm^2, the negative ions appeared (Fig. 6). Energy spectra of negative ions for this intensity shifted to lower energy values. Exponential fitting gives the temperature of $T \sim 140$ eV, which points to the fact that the acceleration by thermal electrons is dominant. The high-energy tail still exists, reflecting the presence of a very small portion of ions accelerated by hot electrons, whose amount and mean energy at an intensity of 10^{15} W/cm^2 are small. The spectra of O and C negative ions behave similarly, but the energies are lower. We did not observe any negative ions of Si with the energy exceeding 100 eV for this intensity.

In order to understand the observed peculiarities of the formation of negative ions we performed the numerical simulation of the ionization kinetics in expanding plasma. Plasma expansion was described with the assumption of the adiabatic

gas expansion into the vacuum [16]:

$$\begin{cases} n = n_0 \frac{D_0 R_0^2}{DR^2} \mathrm{e}^{-\left(\frac{x^2}{D^2}+\frac{r^2}{R^2}\right)}, \\ D\frac{\partial^2 D}{\partial t^2} = \frac{2E}{M}, \\ R\frac{\partial^2 R}{\partial t^2} = \frac{2E}{M}, \\ E = E_0 \left(\frac{D_0 R_0^2}{DR^2}\right)^{\frac{2}{3}}, \end{cases}$$

where n corresponds to the concentration of particles, D and R are respectively the distance from the target and the radius of the plume in cylindrical coordinates and E is the free energy of the plasma (D_0, R_0 and E_0 are the initial plasma parameters). This set of equations was coupled with equations describing kinetics of plasma in the presence of single-charged (positive and negative) ions and neutrals of the identical atomic number. Ionization and recombination rates of positive ions were taken in McWhirter's form [17, 18].

Negative ions can be formed in plasma from neutrals by means of either the photoattachment of an electron [19, 20] or the electron attachment in three-body collisions of a negative ion, electron and neutral [21, 22], while the negative-ion recombination takes place due to the impact recombination during collisions of negative ions with positive ions [23, 24], neutrals [25–27] and electrons [28, 29]. An additional channel of the negative-ion formation is provided by collisions between single-charged positive ions and neutral atoms or molecules of the residual gas [30–32]. We took into account all mentioned processes because their rates strongly depend on plasma properties (temperature, electron concentration, etc.) and energies of colliding particles, and different processes become substantial at different stages of the plasma blow-off evolution.

The consecutive analysis of the negative-ion formation in expanding femtosecond plasma lies beyond the scope of this paper. We will briefly describe the main result of the numerical modeling made for purely hydrogen plasma with the initial density $n_0 = 10^{22}$ cm^{-3}. Figure 7 illustrates the energy spectrum of positive and negative H ions calculated at the same distance from the target as in the performed experiments (see Fig. 6a for comparison). In the numerical simulation, the efficiency of the negative-ion production exceeds 10^{-3}, which is in a reasonable agreement with the experimental data. Bearing in mind this efficiency and assuming that the duration of the ion pulse at the 10-cm distance from the target is $\tau \sim 0.1$–1 μs, we estimate the negative-ion current under our experimental conditions as 100 μA.

Calculations show that collisions with molecules of residual gas play a dominant role in negative-ion formation, at least under our experimental conditions with the residual gas pressure $p \sim 10^{-4}$–10^{-5} Torr and the distance from the detector of 73 cm. For particle energies above 10 keV the coincidence between spectra of negative and positive hydrogen ions in Fig. 7 is evident. The high-energy tail of the energy spectrum of H^- ions declines faster than that for H^+ ions due to the decrease of the cross section of the process of negative-ion formation through collisions with residual gas molecules (mostly N_2). Actually, this cross section reaches its maximum

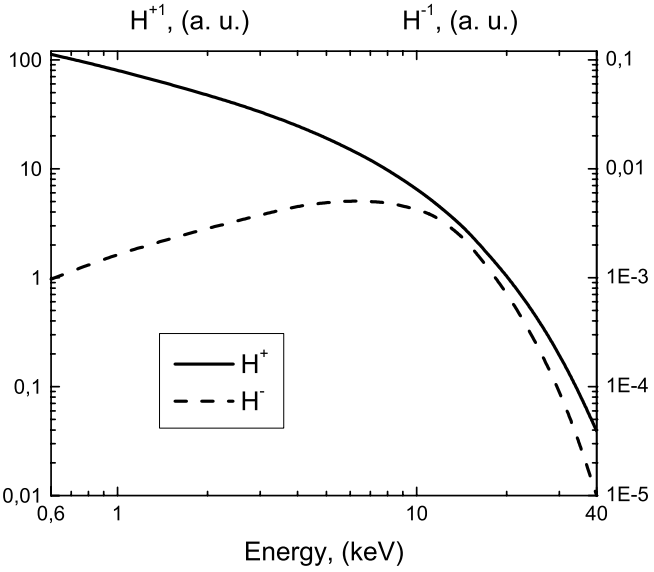

FIGURE 7 Energy spectrum of positive Y^+ and negative Y^- hydrogen ions in expanding laser plasma at 72-cm distance from the target

at the particle energy of about 10 keV both for H^--ion formation from a neutral H atom ($\sigma \sim 10^{-17}$ cm^2) and from a H^+ ion ($\sigma \sim 5 \times 10^{-18}$ cm^2) [30–32]. The same behavior can be observed in experimental data (Fig. 6a).

At the same time, the calculated negative-ion spectrum does not follow the experimental spectrum for energies below 5 keV. This can be explained from the fact that the negative-ion yield strongly depends on the electron concentration. In our calculations with pure hydrogen plasmas the electron concentration was determined on the assumption of the plasma quasineutrality. The assumption of pure hydrogen plasma is valid for the high-energy fraction of plasma rapidly streaming out of the target with velocities above 10^8 cm/s (see Fig. 5a) and becomes inaccurate for the low-energy fraction with expansion velocities below 5×10^7 cm/s. Hydrogen ions of the latter part are accompanied by highly charged positive ions of C, O and Si (see Fig. 5b–d) with the same expansion velocities. Hence, from the assumption of plasma quasineutrality, this fraction of the plasma blow-off has a few times higher electron concentration as compared to that assumed in our model. This, in turn, should lead to the increase of the amount of neutral hydrogen atoms and H^- ions with the subsequent decrease of the amount of H^+ ions, thus making low-energy parts of the spectra of single-charged ions in Fig. 7 closer to each other (see also Fig. 6a).

4 Conclusions

Thus, our experiments revealed a remarkable property of femtosecond laser plasma – the ability to act as a source of fast negative ions with energies of several tens of keV at the laser-pulse intensity $I \sim 2 \times 10^{16}$ W/cm^2. The impurities of H, C and O atoms in the silicon target lead to the production of a great amount of fast positive and negative ions of these atomic species, while Si ions gain less velocity from plasma expansion. The energy spectra of positive and negative ions of the same atomic number are highly correlated due to the fact that most negative ions arise under collisions of positive

single-charged ions and neutral atoms of mentioned species with molecules of the residual gas. This allows one to control the negative ion production rate by adjusting the residual pressure and length of flight of the detected ions.

Our experiments with other targets (Fe, Ti and others) at the same laser-pulse intensity have proved that fast negative ions can be observed if the affinity energy exceeds 0.1 eV. Indeed, for Fe ($E_a = 0.164$ eV) the negative-ion signal was much weaker than that for Si at the same intensity, and for Ti ($E_a = 0.08$ eV) the negative-ion signal was below the detection limit.

At lower laser-pulse intensities (10^{14}–10^{15} W/cm^2) the energy of negative ions is reduced, following the decrease of energy of positive ions. This reduction of the amount of negative ions may occur thanks to the noticeable decrease of cross sections of all processes leading to the formation of negative ions of energies below 2 keV.

Recently, negative ions with energies of up to 70 keV were observed from the CD_4 cluster irradiated by a 10^{18}-W/cm^2 femtosecond laser pulse [33]. It seems to be of special interest to investigate the negative-ion production at sub-relativistic and even relativistic intensities, when the ion energy per unit of charge reaches a few MeV. The decrease of cross sections of all the processes leading to the negative-ion production can be compensated by adjusting the pressure and type of the residual gas or by carrying the ion stream through a gas jet or thin foil.

ACKNOWLEDGEMENTS The authors greatly acknowledge the assistance of Yu. Mikhailova while preparing this work for publication. This research was supported by the Russian Foundation for Basic Research (Project No. 02-02-16659) and ISTC Project No. 2651p.

REFERENCES

1 B.M. Smirnov: *Negative Ions* (McGraw-Hill, New York, London 1982)
2 M.-J. Nadeau, M.A. Garwan, X.-L. Zhao, A.E. Litherland: Nucl. Instrum. Methods B **123**, 521 (1997)
3 G.I. Dimov: Rev. Sci. Instrum. **67**, 3393 (1996)
4 D.G. Koshkarev: Nuovo Cimento **106A**, 1567 (1993)
5 G. Korschinek, T. Henkelmann: Rev. Sci. Instrum. **63**, 2672 (1992)
6 S.V. Latyshev: Tech. Phys. **42**, 828 (1997)
7 G. Korschinek, T. Henkelmann: Nucl. Instrum. Methods A **302**, 376 (1991)
8 Y.A. Bykovskii, V.I. Romanyuk, S.M. Sil'nov: Sov. Tech. Phys. Lett. **14**, 410 (1988)
9 T. Henkelmann, G. Korschinek, M. Paul: Rev. Sci. Instrum. **65**, 1182 (1994)
10 R.V. Volkov, V.M. Gordienko, I.M. Lachko, P.M. Mikheev, B.V. Mar'in, A.B. Savel'ev, O.V. Chutko: JETP Lett. **76**, 139 (2002)
11 R.V. Volkov, V.M. Gordienko, M.S. Djidjoev, M.A. Zhukov, P.M. Mikheev, A.B. Savel'ev, A.A. Shashkov: Quantum Electron. **27**, 1081 (1997)
12 R.V. Volkov, S.A. Gavrilov, D.M. Golishnikov, V.M. Gordienko, P.M. Mikheev, A.B. Savel'ev, A.A. Serov: Quantum Electron. **31**, 241 (2001)
13 N.G. Basov, Y.A. Zakharenkov, A.A. Rupasov: *Diagnostika plotnoi plazmy/Dense Plasma Diagnostics* (Nauka, Moscow 1989)
14 A. Maksimchuk, S. Gu, K. Flippo, D. Umstadter: Phys. Rev. Lett. **84**, 4108 (2000)
15 A.B. Andreev, V.M. Gordienko, A.B. Savel'ev: Quantum Electron. **31**, 941 (2001)
16 Y.B. Zel'dovich, Y.P. Raizer: *Physics of Shock Waves and High-Temperature Hydrodynamic Phenomena*, ed. by W.D. Hayes, R.F. Probstein (Academic Press, New York 1966)
17 R.W.P. McWhirter: *Plasma Diagnostic Techniques* (Academic, New York 1965) p. 210
18 A.C. Kolb, R.W.P. McWhirter: Phys. Fluids **7**, 519 (1964)
19 S. Geltman: Astrophys. J. **136**, 935 (1962)
20 S.J. Smith, D.S. Burch: Phys. Rev. **116**, 1125 (1959)
21 A. Herzenberg: J. Chem. Phys. **51**, 4942 (1969)
22 D. Spence, G.J. Schulz: Phys. Rev. A **5**, 724 (1972)
23 A.A. Radtsig, B.M. Smirnov: JETP **60**, 521 (1971)
24 L.F. Errea, C. Harel, P. Jimeno, H. Jouin, L. Mendez, A. Riera: Phys. Rev. A **54**, 967 (1996)
25 J.C. Browne, A. Dalgarno: J. Phys. B **2**, 885 (1969)
26 D.G. Hummer, R.F. Stebbings, W.L. Fite, L.M. Branscomb: Phys. Rev. **119**, 668 (1960)
27 M.W. Gealy, B. van Zyl: Phys. Rev. A **36**, 3091 (1987)
28 M.S. Pindzola: Phys. Rev. A **54**, 3671 (1996)
29 F. Robicheaux: Phys. Rev. A **60**, 1206 (1999)
30 Ya.M. Fogel, V.A. Ankudinov, R.E. Slabospitskii: JETP **5**, 382 (1957)
31 P.M. Stier, C.F. Barnett: Phys. Rev. **103**, 896 (1956)
32 Y.M. Fogel, V.A. Ankudinov, D.V. Filippenko, N.V. Topolia: JETP **7**, 400 (1959)
33 S.D. Moustaizis, P. Balcou, J.-P. Chambaret, D. Hulin, G. Grillon, J.-P. Rousseau, M. Schmidt: AIP Conf. Proc. **639**, 197 (2002)